Fortgeschrittenen Praktikum II

Mößbauer effect

04.04.2016

Benjamin Winkelmann
Peter Spalthoff

Tutor: Veronika Magerl

Contents

List of Figures

List of Tables

1 Goal of the experiment

By measuring absorption of photons of the $14.4kev$ transition of Fe-57, in stainless steel and natural iron, the isomeric shift, the effective absorber thickness, the Debeye-Waller-factor of the source the lifetime of the excited Fe-57 state, the magnetic field at the location of the nucleus and the magnetic moment of the $14.4ke$V state.

2 physical principles

2.1 Interaction of Gamma radiation with matter

Photons interact with matter in three major ways[2]:

Photoelectric effect

Shell electrons of atoms absorb photons and gain its energy, leaving the potential well of the atom and exiting the shell with the energy $E_e = E_\gamma - E_B$ with E_B being the binding energy of the electron.

Compton scattering

Compton Scattering is the elastic scattering of photons at quasi free electrons ($E_B << E_\gamma$) and its wavelength $\lambda = 2\pi c/\omega$ is shifted, depending on the scattering angle φ(see figure 2.1):

$$\lambda_S - \lambda_0 = \frac{2\pi\hbar}{m_e c}(1 - cos(\varphi)) \tag{2.1}$$

Pair Production

A photon can produce a positron electron pair if it has an energy of at least $2 \cdot m_e = 1.022MeV$ the photon is lost in the processes reducing the Intensity of the photon beam.

Due to those processes the intensity of electromagnetic radiation decreases exponentially with penetration depth d:

$$I(d) = I_0 \cdot exp(-\mu d) \tag{2.2}$$

where μ is the attenuation coefficient.

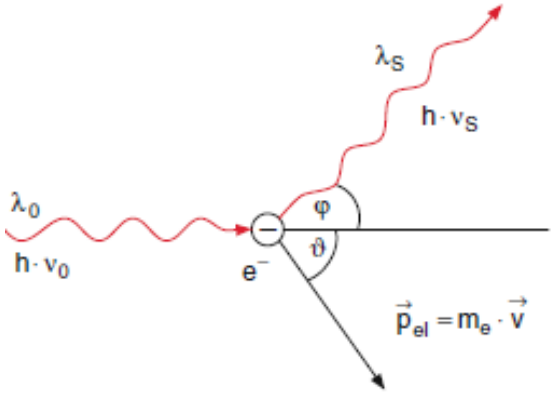

Figure 2.1: Compton effect: A photon is scattered by a (quasi) free electron changing its direction by an angle φ[2]

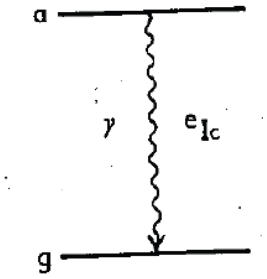

Figure 2.2: principle of spontaneous γ emission of excited nuclei. Transitioning from an excited state (E_a) to the ground state (E_g) the nucleus emits a photon with energy $E_a - E_g = \hbar\dot{\omega}$ or transmits that energy directly to an electron of the atomic shell.[1]

2.2 Gamma Decay and resonance absorption

Nuclei in excited states (energy E_a) can spontaneously transition into the ground (energy E_g) state. The energy ΔE the nucleus loses is either carried by an emitted photon (spontaneous emission) or directly gained by a shell electron (inner conversion).
In the case of spontaneous emission, the photon can be absorbed by a nucleus of the same kind which thereby transits into an excited state. This is called resonance absorption. However due to the recoil the nuclei receive this rarely happens for free atoms. Consider the rest frame of a nucleus, that means its momentum is $p_0 = 0$. Now consider this nucleus decays by emitting a photon. Since the photon carries the momentum

$$p = \frac{E_\gamma}{c} = \frac{\hbar}{c} \cdot \omega \tag{2.3}$$

with the reduced Planck constant $\hbar$ and c the speed of light, and momentum is conserved the nucleus receives a recoil equal to the photons momentum and therefore also kinetic

energy or recoil energy R. The emitted photon therefore has the energy [4]:

$$E_\gamma = \Delta E - \frac{p^2}{2m} = \Delta E - \frac{(\hbar\omega)^2}{2mc^2} =: \Delta E - R \tag{2.4}$$

When the photon is absorbed the same applies: the absorbing nucleus receives the recoil R. This means for a photon to be absorbed, inducing a nuclear transition with ΔE the photon has to have the energy:

$$E_\gamma = \Delta E + R \tag{2.5}$$

In consequence the absorption spectrum is shifted relative to the emission spectrum (see fig 2.3 depending on the recoil energy R.

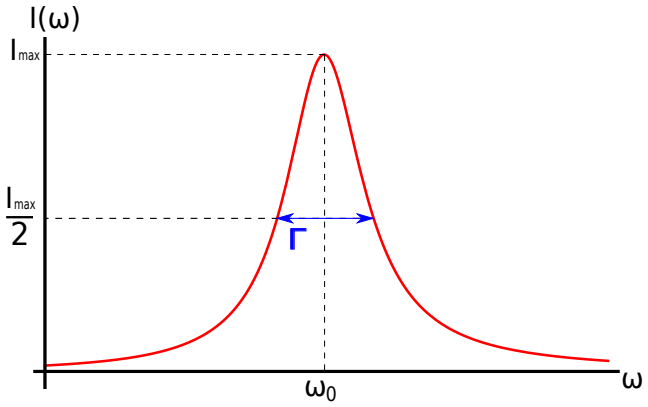

Figure 2.3: Lorentz distribution: $I(\omega) \propto \frac{1}{(\omega-\omega_0)^2+(\Gamma/2)^2}$

2.3 Doppler shift

Due to thermal motion the emitting nucleus and the absorbing nucleus have relative velocity v, shifting the frequency via Doppler effect:

$$E'_\gamma = E_\gamma(1 + \frac{v}{c}) \tag{2.6}$$

So the energy is changed by:

$$E'_\gamma - E_\gamma = E_\gamma \frac{v}{c} \tag{2.7}$$

2.4 Mößbauer effect

The Mößbauer effect is the name for the phenomenon of *recoilless emission* (or absorption). Revisiting equation 2.4 one an see that the recoil energy $R = \frac{(\hbar\omega)^2}{2mc^2}$ is inversely proportional to the mass of the nucleus. In a solid it is possible for the whole lattice the absorb the recoil therefore increasing the recoiled mass enormously, so that $R \approx 0$[1]. This effect means atoms that shows this behavior (In this experiment Fe-57) can emit photons, that can be reabsorbed by atoms of the same kind.

[1] this is a simplified description, for a more detailed one see [4] and [1]

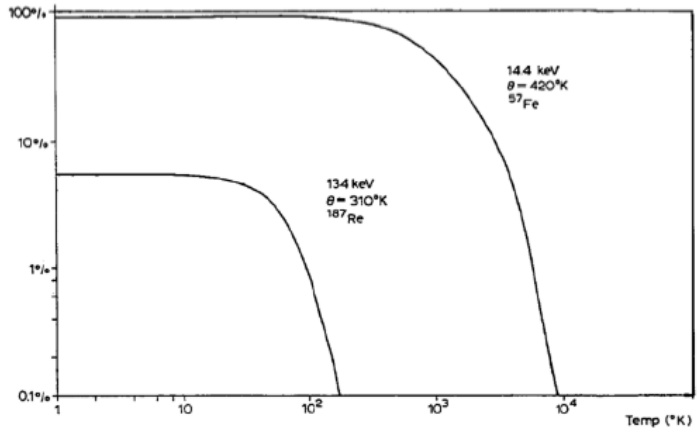

Figure 2.4: Debye factor as a function of temperature in Fe-57 and Re-187. At room temperature Fe-57 has a ratio of recoilless emission absorption of 0.91

2.5 Debye-Waller factor

The Debye-Waller factor is the ratio of recoilless absorption.

$$f = exp\left[-\frac{3R}{2k \cdot \Theta_D}\left(1 + \frac{4T^2}{\Theta_D^2}\int_0^{\Theta/T}\frac{xdx}{e^x - 1}\right)\right] \tag{2.8}$$

Where R is the recoil energy, k the Boltzmann constant, Θ_D the Debye temperature. If the temperature is low $T << \Theta_D$ this can be simplified to:

$$f \approx exp\left[-\frac{3R}{k \cdot \Theta_D}\left(\frac{3}{2} + \frac{\pi^2 T^2}{\Theta_D^2}\right)\right] \tag{2.9}$$

2.6 Isomer shift

Since electrons of an atomic shell are kept within the coulomb potential of the nucleus their potential energy depends on the charge distribution in the nucleus. Transitioning to an excited state affects this distribution therefore also affecting the potential energy of the electrons. This change in energy shifts the frequency that an absorbed photon must have to induce the transition[1].

2.7 Hyperfine splitting

The nucleus has magnetic moment (μ_I) and spin I. In a surrounding magnetic field H the energy level splits into $2I + 1$ sub-energy levels. The sub-sates are characterized by the magnetic quantum number $m_I = -I, I + 1.., I - 1, I$ and the energy difference induced is:

$$E_{HFS} = \frac{\mu_I m_I H}{I} \tag{2.10}$$

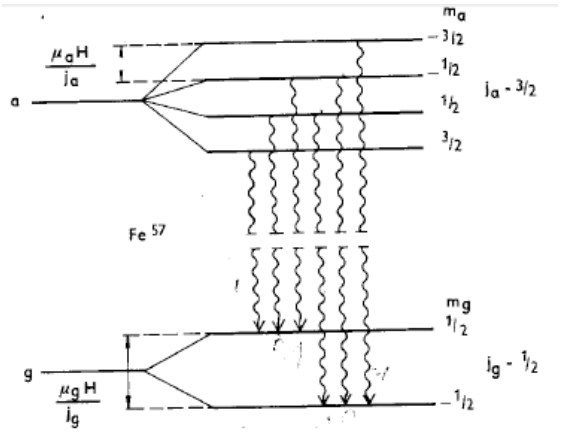

Figure 2.5: Hyperfine splitting for Fe-57 in magnetic field H for the ground state g ($I_g = 1/2$) and the excited state ($I_a = 3/2$).[1]

The transition $m_a \to m_g$ emits photons with energy ω:

$$E_\gamma(m_a, m_g) = E_0 - \left(\frac{\mu_a m_a}{I_a} - \frac{\mu_g m_g}{I_g}\right) H \tag{2.11}$$

3 Experimental setup and procedure

3.1 Method

To measure the absorption spectra of stainless steel and natural iron, we irradiate the samples with the $14.4keV$ γ-radiation emitted by a radioactive source. To vary the frequency a motor is used to move the absorber relative to the source (Doppler shift see 2.7). By repeating this measurement for different absorber velocities a spectrum is recorded.

3.2 Setup

The setup consists of the γ source, the absorber on a track, the motor used to move the absorber at constant speeds relative to the source and as the photon detector a scintillator is used. The light signal of the scintillator turned into an electric signal by a photomultiplier. This signal is amplified and shaped in the amplifier. The amplifier has two exits, one of which is connected to a single channel analyzer (SCA). If the signal pulse is within an adjustable window the SCA sends a standardized signal and enables the linear gate, which is also connected to the amplifier via a delay to ensure simultaneity of the signals. If the linear gate is enabled when it receives a signal from the amplifier it transmits the amplifier signal to the multichannel analyzer (MCA), which is read out with a Computer. The second output of the SCA is connected to a counter, which also can be read out with the Computer.

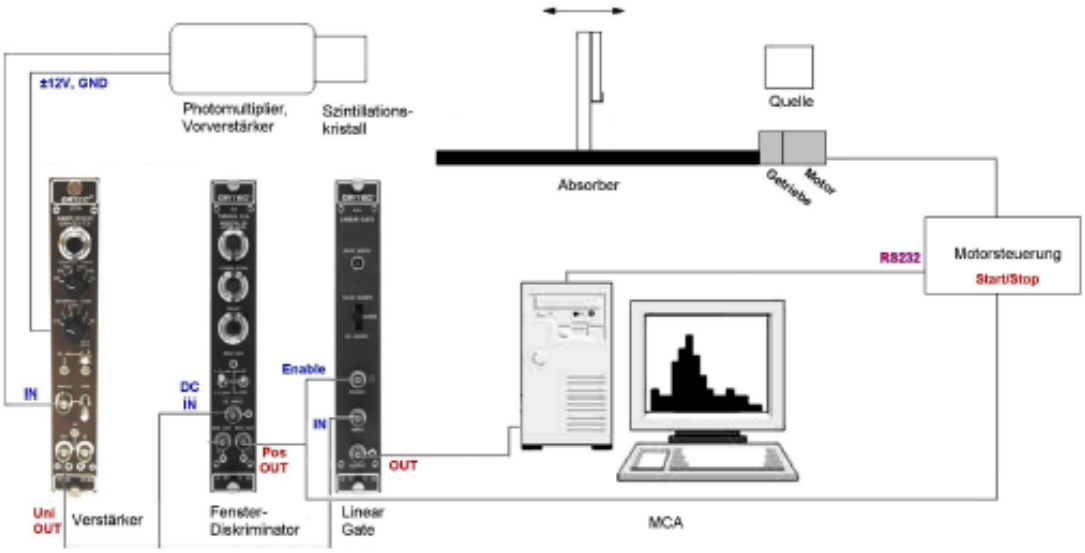

Figure 3.1: Overview of the experimental setup

3.3 The source Co-57

^{57}Co decays via electron capture with a branching ratio of 99.8% and a half life of 270d into an iron in an excited state ^{57}Fe*. This state decays with a half life of 9ns an branching ratio of 88% into the 14.4keV excited state which finally decays to the ground state (Branching ratio for $\gamma - decay$ is 10%) 3.2.

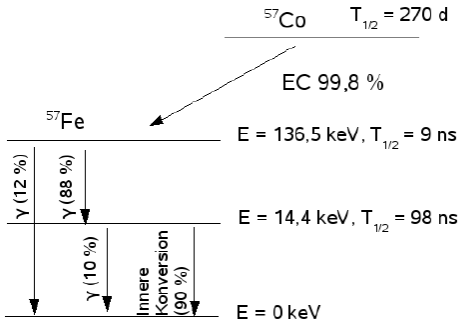

Figure 3.2: Decay series of Cobalt-57

3.4 Americium sample

To calibrate the MCA multiple reference samples are used. For this purpose americium is used as a primary source. The americium is shielded in an stainless steel case with a aperture. Attached in front of this aperture a disc with multiple targets(Cu, Rb, Mo, Ag,

Ba, and Tb) by rotating the disc one can choose a target (see fig 3.3). The radiation of the Americium source excites the target material which in turn starts emitting characteristic x-rays (x-ray fluorescence)[7]. The characteristic lines of the targt samples can be found in fig 3.4 and for the americium source in fig

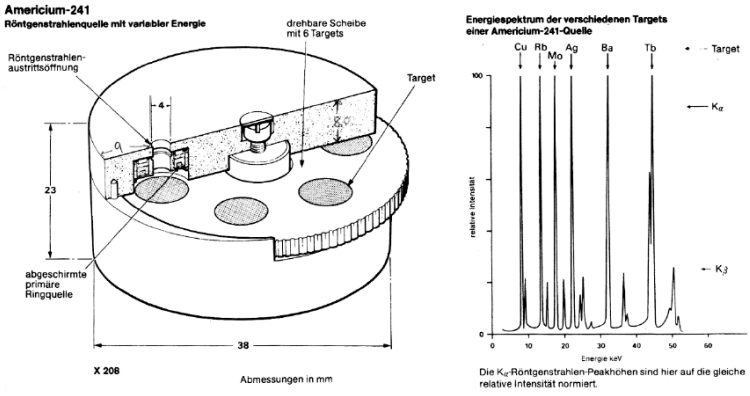

Figure 3.3: Americium sample with target revolver used as reference for the MCA calibration[5]

Target	Energie [keV]		Ausbeute*
	K_α	K_β	$[(\gamma/s)/sr]$
Cu	8,04	8,91	$2,5 \cdot 10^3$
Rb	13,37	14,97	$8,8 \cdot 10^3$
Mo	17,44	19,63	$2,43 \cdot 10^4$
Ag	22,10	24,99	$3,85 \cdot 10^4$
Ba	32,06	36,55	$4,65 \cdot 10^4$
Tb	44,23	50,65	$7,6 \cdot 10^4$

Figure 3.4: K_α and K_β lines of Cu, Rb, Mo, Ag, Ba, and Tb[5]

Energie [keV]	Häufigkeit [%]	Zerfallsmodus
13.927	13.0	L_α-Übergang
17.611	20.2	L_β-Übergang
20.997	5.2	L_γ-Übergang
26.345	2.4	E1-Kernübergang
59.536	35.7	E1-Kernübergang

Figure 3.5: The 5 visible lines of the americium source[7]

3.5 Procedure

3.5.1 MCA calibration

First the window size was set to maximum and the spectrum of the cobalt source was recorded. To identify the 14.4keV peak of the source, the (known) spectra of Cu, Rb, Mo, Ag, Ba, and Tb are measured for 300s each. The results are used to identify the 14.4keV peak in the source spectrum. The Window of the SCA was adjusted accordingly, by recording the source spectrum while adjusting the window and repeatedly resetting the recording on the computer. The Window was then adjusted until only the channels of the $14.4keV$ peak get a signal. We chose the settings:

- upper level: 1.10
- lower level: 0.69

3.5.2 background measurement

The main source of background are photons of the transition between the 136.5keV state and the 14.4kev state (see fig 3.2) being scatter via Compton scattering in the scintillator and falling in the adjusted SCA window. To measure this background, aluminum plates of different thicknesses (measured with) are used to shield the scintillator. For each plate the event counts were measured over 600s. The plate thicknesses were measured with a caliber.

3.5.3 Absorption spectra of stainless steel

First a rough measurement is made: the absorption was measured for velocities of 0.1 mm/s to 1.1 mm/s (both directions) in steps of 0.1mm/s for 180s. For the finer measurements a measuring time of 300s was chosen.

3.5.4 Absorption spectra of natural iron

For natural iron the absorption was measured for absorber speeds between 0.1mm/s and 8mm/s in steps of 0.1mm/s. In a second measurement the range 0.05mm/s to 6.05mm/s was taken, also in steps of 0.1mm/s. The measuring for each velocity was 300s.

3.5.5 Attenuation through acrylic glass

The absorber is removed from the setup at the counting rate measured for 900s, once with acrylic glass and once without.

4 Analysis

4.1 Identifying the Fe-57 transition peak

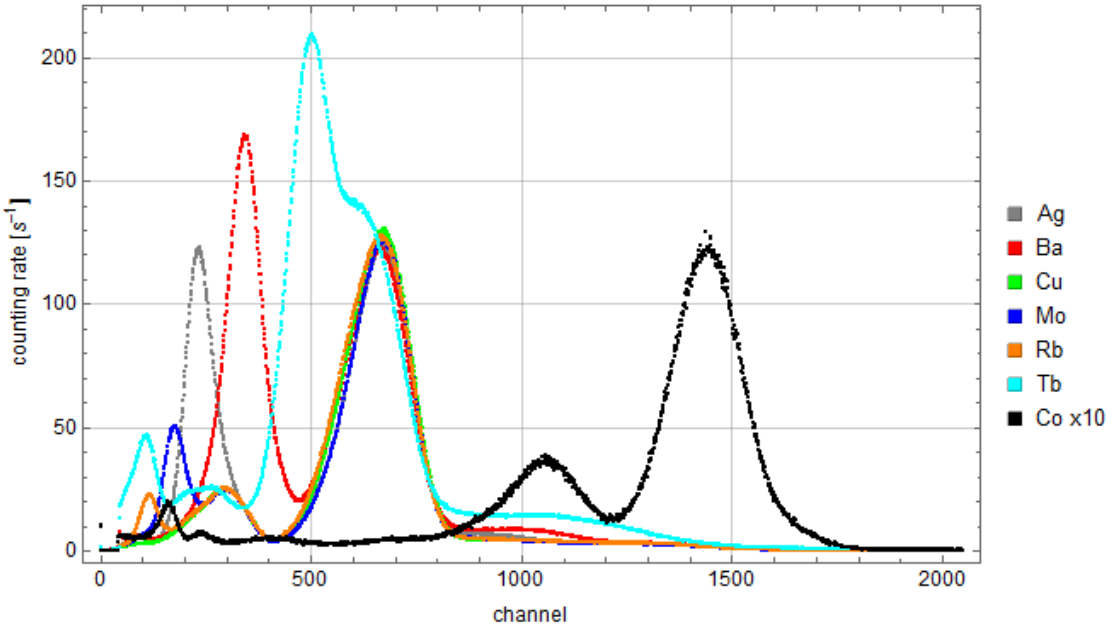

Figure 4.1: Plot of all recorded reference spectra and the cobalt source (upscaled by factor 10 for better comparability)

Around channel 700 all target samples have clearly defined peak. For Terbium(Tb) this peaks blends with its K-line. This peak is caused by photons of the americium source, passing through the targets without interacting. The K_α-line of copper (Cu) is beyond the left edge and therefore not meassured. The peak positions are estimated from the fig 4.1. The error is estimated to be $s_{Ch} = 10$. The Result can be seen in table 4.1. One can already identify the peak since it has to lie between the Rb-peak and the Mo-peak, which is suggesting the peak furthest to the left (around channel 160) belongs to the 14.4keV line.

traget	energy [keV]	peak channel
Cu	8.04	-
Rb	13.37	120
Mo	17.44	180
Ag	22.10	230
Ba	32.06	340
Tb	44.23	500

Table 4.1: number of the channel for the K-line peaks

The Linear function $E(ch) = a \cdot ch + b$ was fitted to the data see figure

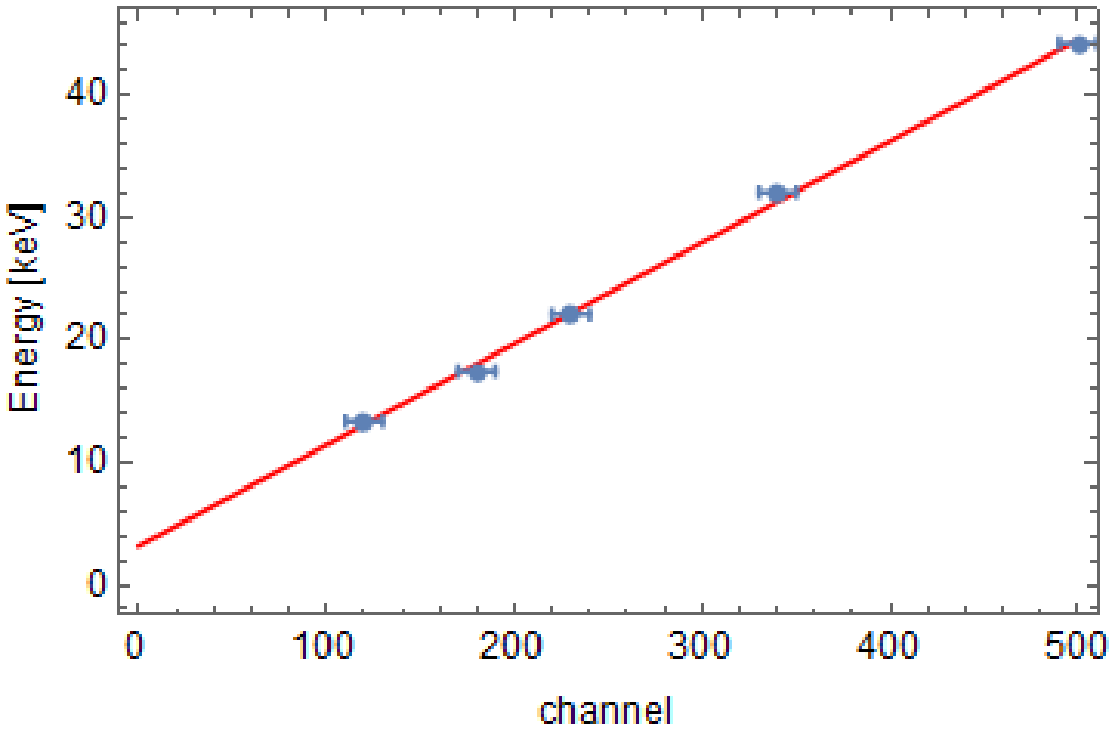

Figure 4.2: Linear fit for the calibration of the MCA

The results are:

$$\begin{aligned} a &= (0.083 \pm 0.002) keV \\ b &= (3.2 \pm 0.6) keV \end{aligned} \tag{4.1}$$

The position of the 14.4keV peak should be at[2]:

$$ch_{14.4keV} = \frac{14.4keV - b}{a} = 135 \pm 4 \tag{4.2}$$

A Comparison with figure 4.1 shows that the peak furthest to left is the closest ($ch = 160 \pm 10$)to this value, however the values lie more almost two standard deviations apart. Fortunately, an exact calibration is not needed for further analysis.

4.2 Compton

High energy photons such as those from the transitions with 122 keV and 136 keV lose energy when passing through matter via the Compton effect. Some of these photons will

[2] error calculated according to gaussian error propagation. Unless specified otherwise, all errors of values calculated with other values are determined this way

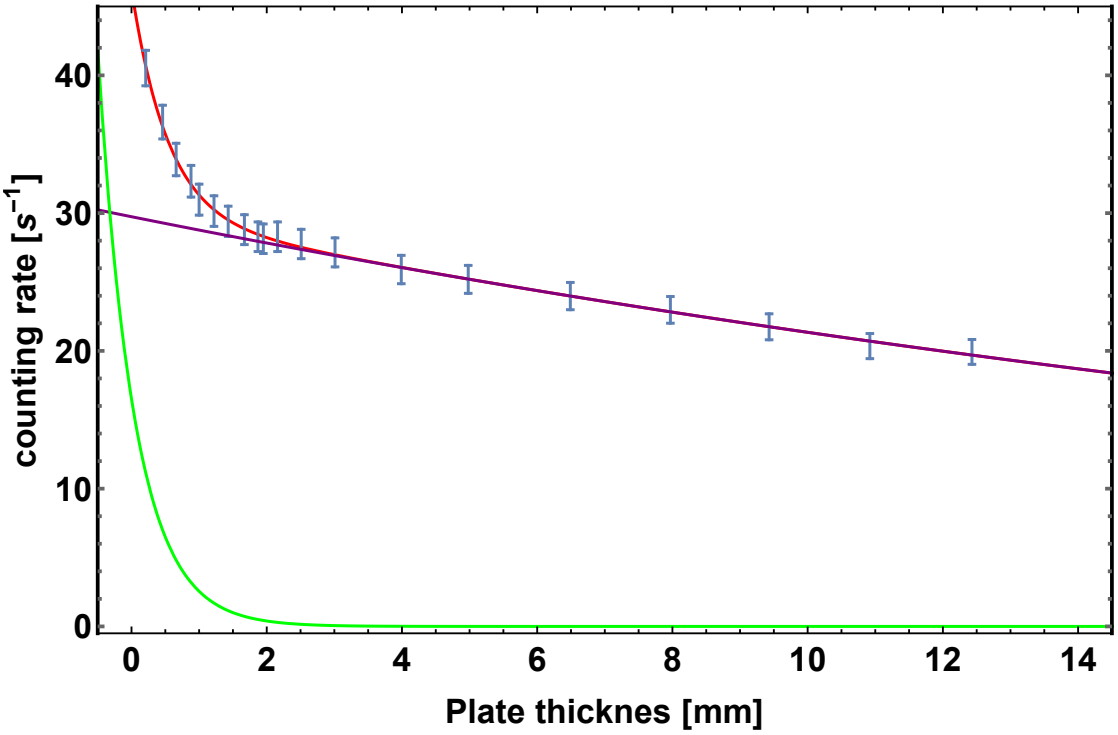

Figure 4.3: The compton background data along with the fitted sum of the two exponential functions in red. The curve for Compton underground is colored purple and that for the 14, 4 keV photons green.

randomly fall within the energy windows that was set for the measurements and thus pose an underground that needs to be subtracted from the data for parts of the further analysis. Since higher energy photons lose their energy slower than lower energy photons when passing through matter, one can separate the two by placing aluminum plates in the beam with a range of thicknesses. The count rate decreases exponentially with the thickness d

$$\dot{N} = \dot{N}_0 e^{-\mu d} \tag{4.3}$$

measurements were taken for absorber thicknesses between $d = 0.21\,\text{mm}$ and $d = 12.43\,\text{mm}$, which were measured with a caliper to such high precision that the error is far smaller than the Poisson error on the count rates and is thus neglected. Figure 4.3 shows the measured data. As two processes with different speeds, μ_C of the Compton background and μ_0 of the actual data, are expected, the fit function for the count rates for varying absorbers is

$$\dot{N}(d) = A_C \cdot e^{-\mu_C d} + A_0 \cdot e^{-\mu_0 d} \tag{4.4}$$

The resulting fit parameters for the Compton underground were

$$A_C = (29.74 \pm 0.17)\ \mathrm{s}^{-1} \tag{4.5}$$

$$\mu_C = (0.0331 \pm 0.0009)\ \mathrm{mm}^{-1} \tag{4.6}$$

As no aluminum plates are used during regular measurements, the value for $d = 0$, and thus the fit parameter A_C, is the underground rate to be deducted from future measurements.

4.3 Attenuation of the acrylic glass

The acrylic glass in which the sample is cased absorbs some of the radiation. To quantify this, a plate of acrylic glass of roughly the same thickness as the one used to case the sample can be but into the beam. One measurement is taken with the plate and one without. The thickness of the plate was measured as $d = (1.94 \pm 0.01)$ mm. The resulting count rates were

$$\dot{N}_0 = (107.4 \pm 0.3)\ \mathrm{s}^{-1} \tag{4.7}$$

$$\dot{N}_A = (84.8 \pm 0.3)\ \mathrm{s}^{-1} \tag{4.8}$$

where the uncertainties stem from the Poisson errors on the number of counts. The attenuation coefficient can then be calculated:

$$\mu_{acr} = Log\left[\frac{\dot{N}_0}{\dot{N}_A}\right] \cdot \frac{1}{d} = (1.21 \pm 0.02)\ 1/\mathrm{cm} \tag{4.9}$$

With the values given for the attenuation coefficient $\mu/\rho = 1.101\ \mathrm{cm}^2/\mathrm{g}$ and the density of the acrylic glass $\rho = 1.19\ \mathrm{g/cm}^3$ in [5], the mass attenuation coefficient can also be calculated as $\mu = 1.31019\ 1/\mathrm{cm}$. Clearly, this value is in disagreement with the one calculated from the measurements. With this value as well as the thickness of the plate, the count rate after the acrylic glass can also directly be calculated from the count rate without the acrylic glass as

$$\dot{N}_A^{calc} = \dot{N}_0 \cdot e^{-\mu d} = (83.3 \pm 0.3)\ \mathrm{s}^{-1} \tag{4.10}$$

The two values agree only with their 2σ intervals. The literature value $\mu/\rho = 1.101\ \mathrm{cm}^2/\mathrm{g}$ is actually listed for energies of $E_\gamma = 15$ keV, which is slightly more than the that of the 14.4 keV transition. However, the value is higher for lower energies, which means that using a value for the exact energies of the photons in this experiment would lead to an even lower calculated count rate. The cause for the disagreement of the values is thus likely that the thicknesses of the plates do no match. A quick calculation reveals that a disagreement of 5% would bridge the gap and have the values agree within their 1σ intervals.

4.4 Single line absorber

The results for the measurement of the absorption spectrum of stainless steel can be seen in figure 4.4. To evaluate the data a voigt function (convolution of a Gaussian and Lorentz) was fitted to it:

$$f(v) = B - A \cdot Voigt((v - v_0), \delta, \sigma) \tag{4.11}$$

where v is the absorber velocity, v_0 the peak position, δ is the

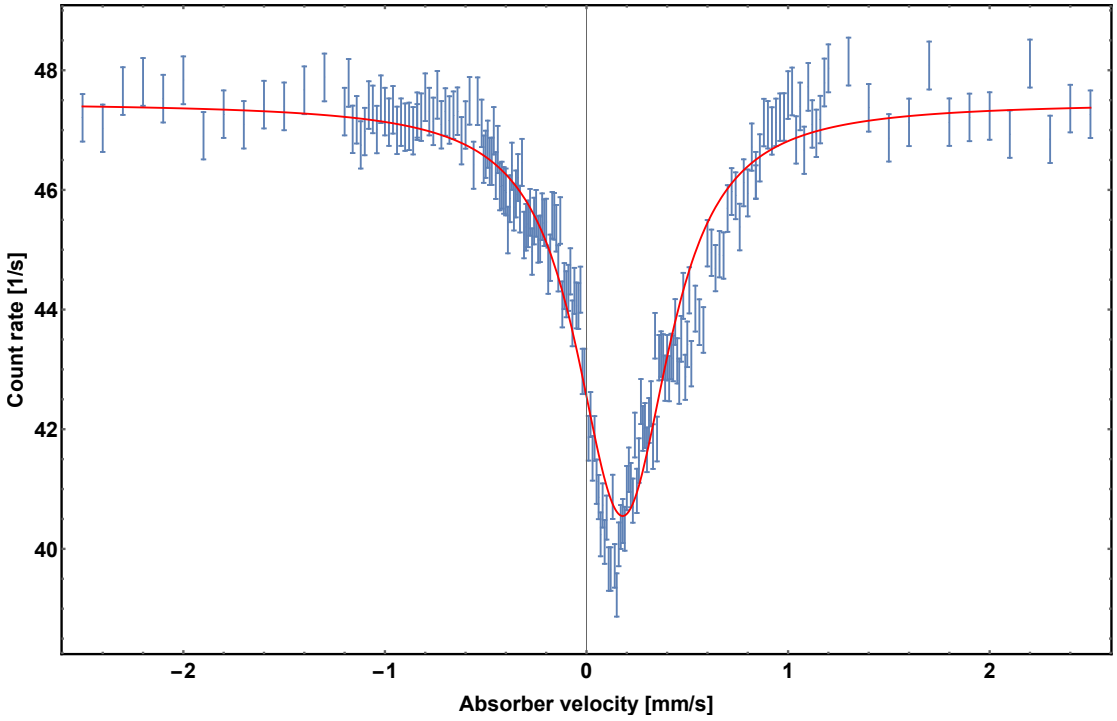

Figure 4.4: Measured absorption spectrum for stainless steel and Voigt fit.

The fit results are:

	Estimate	Standard Error
v_0	0.179	0.005
σ	0.25	0.03
δ	0.14	0.10
B	47.46	0.11
A	5.8	0.4

The fit function exhibits notable differences from the data. The data peak lies about $unit 0.05 mm/s$ closer to zero than the Voigt peak and there is a noticeable asymmetry. The left flank is steeper than the right. This is a hint that the model does not reflect the data fully.

4.4.1 Isomeric shift

Since the background is constant it only effects variable B of the fit function, therefore with the parameter v_0 one can calculate the isomeric shift, without having to correct for the background. 2.7:

$$E_{iso} = (8.61 \pm 0.24) \cdot 10^{-9} eV \tag{4.12}$$

4.4.2 Effective absorber thickness

The effective absorber thickness is given by [5]:

$$T_A = f_A n_A \beta \sigma_0 d_A \tag{4.13}$$

where $d_A = 25\mu m$ is the absorber thickness, n_A is the number of iron atoms per volume, $\beta = 0.022$ the ratio of Fe-57 in the isotope mixture, σ_0 the cross section and $f_A = 0.8$ the Debye-Waller-factor of the absorber. To calculate n_A literature values are used ([8]):

$N_A = 6.022 \cdot 10^{23} mol^{-1}$	Avogadro constant
$\rho_{Fe} = 7.874 g/cm^3$	density of iron
$A_Fe = 55.845 g/mol$	molar mass of iron
$r = (0.70 \pm 0.05)$	fraction of iron in the absorber[5]

The number of Fe atoms per volume is then given by:

$$\frac{\rho_{Fe}}{A_Fe} N_A \cdot r = (5.9 \pm 0.4) \cdot 10^{22} cm^{-3}$$

The absorption cross section is given by [1]:

$$\sigma_0 = \frac{\lambda^2}{2\pi} \left(\frac{2I^* + 1}{2I + 1} \right) \frac{1}{1 + \alpha} \tag{4.14}$$

where $\alpha = 9$ (see [1]) is the conversion coefficient, λ the wavelength of the absorbed photon, $I^* = 3/2$ and $I = 1/2$ are the nuclear spins of the excited and ground state. With $\lambda = \frac{hc}{E_\gamma} = 86.14 pm$, the cross section is:

$$\sigma_0 = 2.36 \cdot 10^{-} 22 m^2 \tag{4.15}$$

Plugging those values in equation 4.13, the effective absorber thickness is:

$$T_A = (6.2 \pm 0.4) \tag{4.16}$$

4.4.3 Debye Waller factor of the source

The Debye-Waller-factor is related to the count rate with no absorption $Z(\infty)$, the minimal count rate $Z(v_min)$ (maximal absorption) and the effective absorber thickness T_A [1]:

$$\frac{Z(\infty) - Z(v_{min})}{Z(\infty)} = f \cdot [1 - exp(-\frac{T_A}{2}) J_0(\frac{iT_A}{2})] \tag{4.17}$$

i is the imaginary unit and J_0 the order zero Bessel function. The count rates on the left can be determined from the fit function $f(v)$ and the Compton background A_C:

$$\begin{aligned} Z(\infty) &= B - A_C \\ Z(v_{min}) &= A - A_C \end{aligned} \tag{4.18}$$

Rearranging equation 4.17 we get for the Debye-Waller factor of the source

$$f_s = 0.51 \pm 0.08 \tag{4.19}$$

The rather big error (15%) is mainly caused by the uncertainty of $Z(v_{min})$ since all errors of the fit function parameters contribute.

4.4.4 Life time of the 14.4keV state

From the fit

From the Voigt fit the half width $\delta = 0.14 \pm 0.10$ of the convoluted Lorentzian can be extracted. It has to be noted, that δ from the fit is still in units of velocity (mm/s), so using equation 2.7 the wanted half width Γ is:

$$\Gamma = 6.2 \pm 4.6 \cdot 10^{-8} \text{ eV} \tag{4.20}$$

With Heisenberg's uncertainty relation $\Gamma \cdot \mathcal{T} = \hbar$, the mean life time is:

$$\mathcal{T} = (11 \pm 8) ns \tag{4.21}$$

The fit uncertainty propagates through the calculation and is responsible for the relative error of over 70%. Despite of this the literature value $\mathcal{T}_{lit}$=141ns is still more than seven standard deviations away from the determined value.

From the effective absorber thickness

The relative line broadening $\Gamma_a/2\Gamma$ is determined graphically from figure 4.5. For this purpose the program Inkscape was used. By measuring the length of each coordinate axes in pixels, factors are determined, allowing the conversion between line lengths in pixels and their corresponding values.

The effective absorber thickness was calculated in section 4.4.2. To estimate the error, the relative broadening was also determined for $T_A \pm s_{T_A}$. The results are:

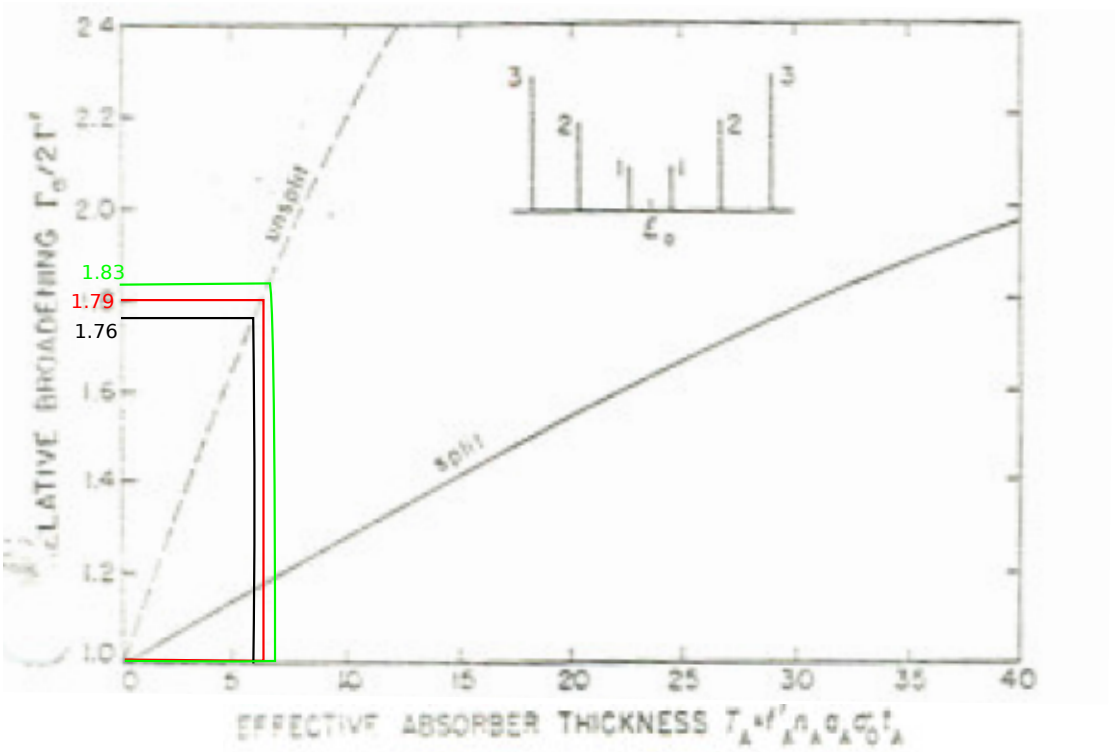

Figure 4.5: Graphical determination of the relative line broadening[9]

T_A	$\frac{\Gamma_a}{2\Gamma}$
5.8	1.76
6.2	1.79
6.6	1.83

Table 4.2: relative broadening for different absorber thicknesses

For the error estimation the bigger difference (0.04) is chosen. As the peak width of the absorber, the width of the fitted Voigt profile is used, calculated with an empirical approximation(0.02% accuracy)[12]:

$$\Gamma_a = 0.5 \cdot (1.0692 \cdot \delta + \sqrt{0.86639 \cdot \delta^2 + 4 \cdot (2\sigma\sqrt{2ln(2)})}) \tag{4.22}$$

and with the values from the Voigt fit for δ and σ

$$\Gamma_a = (32 \pm 4) \text{ neV} \tag{4.23}$$

and

$$\Gamma = (8.9 \pm 0.6) \text{ neV} \tag{4.24}$$

Due to the time-energy uncertainty the mean life time is then given by:

$$\mathcal{T} = \hbar/\Gamma = (6.5 \pm 0.4) \text{ ns} \tag{4.25}$$

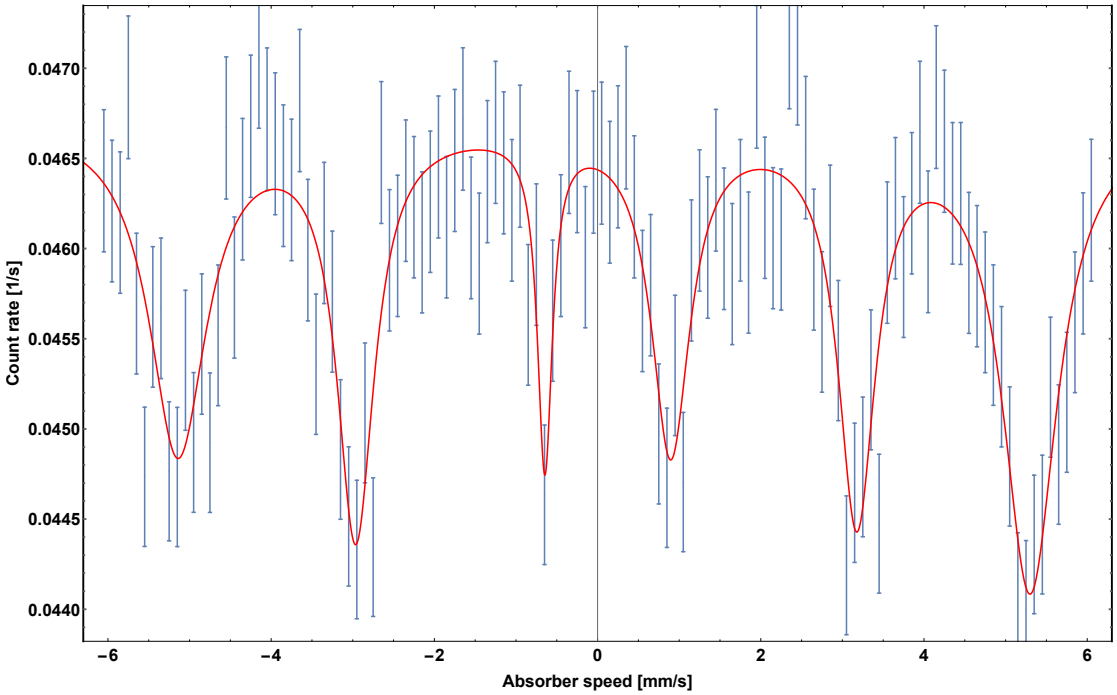

Figure 4.6: The six-line absorber spectrum. A sum of 6 Lorentz functions was fitted to the data.

4.5 Six-line absorber

Figure 4.6 shows the measurement results of the six-line absorber measurements. A sum of 6 Lorentz function, one for each peak, was fitted to the data. Gauss functions are to wide and due to the large uncertainties and the relatively low number of points per peak, the effort of doing Voigt fits is not warranted. The Lorentz fit describes the data well enough, with a χ^2 value of 1.0. The peak positions and the corresponding energy shifts are listed in table 4.3.

4.5.1 Isomeric shift

As the isomer shift is the offset from 0, three values can be determined here. One for the shift when comparing the first and sixth peak, on for the second and fifth and one for the third and forth. The weighted means of the values listed in table 4.4 are

$$\overline{v}_{iso} = (0.102 \pm 0.024)\ \text{mm/s} \tag{4.26}$$

$$\overline{E}_{iso} = (4.9 \pm 1.1)\ \text{neV} \tag{4.27}$$

which both include their literature values $v_{iso}^{lit} = 0.11$ mm/s and $E_{iso}^{lit} = 5.3$ neV from the data sheet of the sample in their relatively large 1σ intervals.

Peak i	v_i [mm/s]	ΔE [neV]
1	-5.14 ± 0.05	-246.9 ± 2.4
2	-2.96 ± 0.03	-142.4 ± 1.6
3	-0.65 ± 0.03	-31.0 ± 1.4
4	0.90 ± 0.04	43.0 ± 2.0
5	3.18 ± 0.03	152.5 ± 1.6
6	5.30 ± 0.03	254.6 ± 1.7

Table 4.3: Positions of the peaks in the six-line absorber velocity spectrum.

Peaks	v_{iso} [mm/s]	E_{iso} [neV]
6-1	0.08 ± 0.03	3.8 ± 1.5
5-2	0.106 ± 0.023	5.1 ± 1.1
4-3	0.125 ± 0.025	6.0 ± 1.2

Table 4.4: Isomer shifts of the six-line absorber.

4.5.2 Magnetic moment

Equation 2.11 yields

$$E_i = E_{iso} - E_{HFS} = E_{iso} - \left(\frac{\mu_e m_e}{Ie} + \frac{\mu_g m_g}{I_g} \right) \cdot B \tag{4.28}$$

which can be written using the velocities

$$v_i = v_{iso} - \frac{c}{E_0} \left(\frac{\mu_e m_e}{Ie} + \frac{\mu_g m_g}{I_g} \right) \tag{4.29}$$

The nuclear spins are$I_g = 1/2$ and $I_e = 3/2$. Table 4.5 shows the magnetic quantum numbers that correspond to the peaks. The formulas still contain the unknown magnetic

Peak	m_e	m_g
1	$3/2$	$1/2$
2	$1/2$	$1/2$
3	$-1/2$	$1/2$
4	$1/2$	$-1/2$
5	$-1/2$	$-1/2$
6	$-3/2$	$-1/2$

Table 4.5: The magnetic quantum numbers corresponding to the peaks.

field. One can now calculate the velocity differences of the corresponding peaks

$$\Delta v_a = v_6 - v_1 = \frac{2c}{E_0}\left(\mu_g - \mu_e\right) B \tag{4.30}$$

$$\Delta v_b = v_5 - v_2 = \frac{2c}{E_0}\left(\mu_g - \frac{\mu_e}{3}\right) B \tag{4.31}$$

$$\Delta v_c = v_4 - v_3 = \frac{2c}{E_0}\left(\mu_g + \frac{\mu_e}{3}\right) B \tag{4.32}$$

With these three variables, there are three possible combinations to get formulas for the magnetic moment of the excited state.

$$\frac{\Delta v_a}{\Delta v_b} = \frac{\mu_g - \mu_e}{\mu_g - \frac{\mu_e}{3}} \tag{4.33}$$

$$\frac{\Delta v_b}{\Delta v_c} = \frac{\mu_g - \mu_e}{\mu_g + \frac{\mu_e}{3}} \tag{4.34}$$

$$\frac{\Delta v_c}{\Delta v_a} = \frac{\mu_g + \frac{\mu_e}{3}}{\mu_g - \frac{\mu_e}{3}} \tag{4.35}$$

The magnetic moment of the ground state is given in [10] as $\mu_g = (0.09044 \pm 0.0007) \cdot \mu_N$, where the nuclear magneton is $\mu_N = 3.152 \cdot 10^{-8}$ eV/T. Solving these separate formulas for the magnetic moment of the excited state and applying standard Gaussian error propagation yields (in units of μ_N)

$$\frac{\Delta v_a}{\Delta v_b} \Rightarrow \mu_e = \mu_g \frac{3\Delta v_a - \Delta v_b}{\Delta v_a - 3\Delta v_b} = (-0.146 \pm 0.005)\ \mu_\mathrm{N} \tag{4.36}$$

$$\frac{\Delta v_b}{\Delta v_c} \Rightarrow \mu_e = 3\mu_g \frac{\Delta v_c - \Delta v_b}{\Delta v_c + \Delta v_b} = (-0.162 \pm 0.003)\ \mu_\mathrm{N} \tag{4.37}$$

$$\frac{\Delta v_c}{\Delta v_a} \Rightarrow \mu_e = \mu_g \frac{\Delta v_c - \Delta v_a}{\Delta v_a/3 + \Delta v_c} = (-0.160 \pm 0.003)\ \mu_\mathrm{N} \tag{4.38}$$

Stone [10] lists the magnetic moment of the excited state as $\mu_e = (-0.1549 \pm 0.0002)\ \mu_\mathrm{N}$. All values enclose this value at least in their 3σ intervals.

4.5.3 The magnetic field at the nucleus

With the magnetic moments known, the magnetic fields can now be calculated from the formulas in equation 4.32

$$B_a = (33.7 \pm 0.7)\ \mathrm{T} \tag{4.39}$$

$$B_b = (32.4 \pm 0.4)\ \mathrm{T} \tag{4.40}$$

$$B_c = (31.7 \pm 1.5)\ \mathrm{T} \tag{4.41}$$

which are all within 2σ of the literature value $B_{lit} = 33$ T [11].

5 Summary

5.1 Calibration

5.2 Background

By measuring the absorption for different thicknesses of aluminum, the background count rate was determined to be:

$$A_C = (29.74 \pm 0.17) s^{-}1$$

5.3 Attenuation by the acrylic glass

The attenuation coefficient for the acrylic glass was measured, with the result:

$$\mu_{acr} = (1.21 \pm 0.02)\ 1/\text{cm}$$

The value contradicts the calculated one $\mu = 1.31019$ 1/cm. For the later nominal values for E_γ=15 keV were used which is slightly higher then the energy of the iron transition. Their difference can be explained by different thicknesses of the glass for the absorber and the empty acrylic glass plate. A 5% disagreement would suffice.

5.4 Single line absorber

The isomeric shift was measured

$$E_{iso} = 8.61 \pm 0.24 \cdot 10^{-9}\ \text{eV}$$

. With the calculated effective absorber thickness $T_A = (6.2 \pm 0.4)$ the Debye-Waller factor of the source was determined:

$$f_s = 0.51 \pm 0.08$$

Both measurements of the mean life time of the 14.4 keV state, namely τ=(11 ± 8) ns (directly from a fit parameter) and τ=(6.5 ± 0.4) ns are far lower than the literature value $\tau_{lit} = 140$ ns.

5.5 Six line absorber

By fitting the sum of six Lorentz curves to the recorded spectrum of natural iron, the following values were determined during evaluation.

Quantity	Value
$\overline{E_{iso}}$	(4.9 ± 1.1) neV
$\mu_e a$	$(-0.146 \pm 0.005)\ \mu_\mathrm{N}$
$\mu_e b$	$(-0.162 \pm 0.003)\ \mu_\mathrm{N}$
$\mu_e c$	$(-160 \pm 0.003)\ \mu_\mathrm{N}$
B_a	(33.7 ± 0.7) T
B_b	(32.4 ± 0.4) T
B_c	(31.7 ± 1.5) T

Table 5.1: Summary of the results for the six line absorber

The isomeric shift lies within one standard deviation at the literature $E_{iso}^{lit} = 5.3$ neV value. The measured values for the magnetic moment enclose the literature value $\mu_e(-0.1549 \pm 0.002)$[10] within their 3σ intervals.

6 References

[1] Wegener, Horst. "Der Mößbauer Effekt und seine Anwendungen". Mannheim 1966

[2] Demtröder, Wolfgang. Experimentalphysik 3 Atome, Moleküle und Festkörper

[3] Jakobs, Karl. Experimentelle Methoden der Teilchenphysik. Vorlesungsskript 2014

[4] Eyges, Leonard. Physics of the Mössbauer effect. 1965

[5] A.Zwerger(2007), S.Winkelmann(1/2011), M.Köhli (2/2011). Versuchsanleitung Fortgeschrittenen Praktikum Teil II - Der Mößbauer-Effekt. 2012

[6] M.Köhler(8/2010), M.Köhli (4/2011). Versuchanleitung Fortgeschrittenen Praktikum Teil I - Kurze Halbwertszeiten

[7] U.Landgraf. Eichspektrum der Americium-Quelle (1997)

[8] https://www.webelements.com/ (28.4.2016)

[9] S. Margulies, P. Debrunner, H. Frauenfelder. Transmission and line broadening in the Mössbauer effect II. 1962

[10] Stone, N.J. *Table of Nuclear Magnetic Dipole and Electric Quadrupole Moments.* Oxford Physics.

[11] Fultz, Brent.*Moessbauer Spectrometry in Characterization of Materials.* John Wiley. New York, 2011.

[12] J.J.Olivero, R.L. Longbothum. Empirical fits to the voigt line width: A brief review. 1997. http://www.sciencedirect.com/science/article/pii/0022407377901613